Supplement of

A global model simulation of present and future nitrate aerosols and their direct radiative forcing of climate

Correspondence to : D. A. Hauglustaine (didier.hauglustaine@lsce.ipsl.fr)

Model description

Free ammonia is used for the neutralization of nitric acid to ammonium nitrate aerosol following the equilibrium reaction:

$$HNO_3 + NH_3 \leftrightarrow NH_4NO_3 \quad (1)$$

The equilibrium constant (K_p) of (1) strongly depends on relative humidity and temperature. The parameterization used for this dependence is based on Mozurkewich (1993). First, the deliquescence relative humidity (DRH, %) is calculated based on Seinfeld and Pandis (1998):

$$DRH = \exp(723.7/T + 1.6954) \quad (2)$$

where T is the air temperature (K). For relative humidities lower than DRH, $K_p = K_{pd}$ and is calculated with:

$$K_{pd} = \exp[118.87-24084/T-6.025 \ln(T)] \quad (3)$$

For relative humidities higher than DRH, $K_p = K_{ph}$ and depends on both temperature and relative humidity (RH) and is calculated based on :

$$K_{ph} = K_{pd} (p_1 - p_2 RH_1 + p_3 RH_1^2) RH_1^{1.75} \quad (4)$$

With RH_1 defined as (1-RH/100) and p_1, p_2, and p_3 provided by:

$$p_1 = \exp[-135.94+8763/T+19.12 \ln(T)] \quad (5)$$

$$p_2 = \exp[-122.65+9969/T+16.22 \ln(T)] \quad (6)$$

$$p_3 = \exp[-182.61+13875/T+24.46 \ln(T)] \quad (7)$$

Model evaluation

Box model simulations

In order to evaluate the thermodynamic nitrate aerosol module developed and used in INCA, we have developed a box model version and used it as a stand-alone version to be evaluated against the ISORROPIA reference model (Nenes et al., 1998). Both the INCA box model and ISORROPIA are constrained by the same input parameters. The input parameters are then varied in order to compare the behavior of the two models across the range of variation in key

inputs (i.e., total sulfate TS, total ammonia TA, total nitrate TN, relative humidity RH, and temperature T). The reference input parameters for all simulations are : T = 280K, RH = 0.9, TS = 2 μg/m^3, TA = 4 μg/m^3, and TN= 5 μg/m^3. Figure S1 shows the evolution of the simulated NO_3^- and NH_4^+ equilibrium concentrations when these parameters are varied separately over a given interval and compares the output to the ISORROPIA results. Overall an excellent agreement is obtained between the INCA module and ISORROPIA. The sensitivity of the two models to key environmental parameters as encountered in the global atmosphere are very similar and the simulated concentrations in close agreement. The major disagreement we note is at sulfate concentrations larger than about 10 μg/m^3 for which the INCA module forms ammonium sulfate preferentially and hence significantly underestimates the ammonium nitrate levels compared to ISORROPIA. This disagreement has no effect on the simulated global concentrations since sulfate concentrations larger than 10 μg/m^3 are essentially not reached in the global model. It should also be pointed out that at temperature higher than about 295K, the volatilization of ammonium nitrate is too efficient and the concentration simulated with INCA drops more rapidly to zero than in ISORROPIA. This limitation has to be kept in mind but even under a warming climate these high temperatures are not often reached in regions concerned by fine particulate nitrate formation or only occasionally and will have a minor impact on the model results.

Diurnal variations

Nitrate aerosols have the ability to dissociate back into the gas phase. As illustrated by Dall'Osto et al. (2009), this means that nitrates have a pronounced diurnal cycle and spend most of the daytime in the gas phase. The detailed evaluation of the diurnal cycle is out of the scope of the use of a global model and of this paper. However, since this diurnal variation has an impact on the radiative forcing, we illustrate in Figure S2 the simulated diurnal variation of nitrate concentrations at four different sites for the period 1/8/2009 to 30/10/2009. A very pronounced diurnal cycle is indeed calculated over the Po Valley or over China. The minimum in NO_3^- concentrations occur during daytime as expected and are often close to zero during that period. This minimum coincides with a maximum in HNO_3 concentrations (not shown) suggesting that volatilization of nitrate particles indeed occurs as indicated by Dall'Osto et al. (2009). In England, the nitrate concentrations and their variation are in agreement with the range of about 0-12 μg/m^3 and variability measured by Dall'Osto et al. (2009) in October 2006. The variability of NO_3 in the model can be explained by a combination of the diurnal cycle associated with the thermodynamic equilibrium of nitrate

formation, superimposed on a variability associated with changing meteorological conditions and transport of pollution episodes from the continent. High pollution episodes of nitrate particles are also simulated in the Netherlands where NH_3 concentrations reach more than 10 $\mu g/m^3$.

Present-day nitrate column

Figure S3 shows the three components of the total nitrate column and shows the fine mode, coarse mode on dust and coarse mode on sea-salt separately. This figure clearly shows that fine nitrate particles associated with anthropogenic emissions contribute to a large extent to the maximum calculated in the central US, in Northern Europe and over the Po Valley, in Northern India and in China. Over Africa, Saudi Arabia, Central Europe and in Northern China, nitrates on dust contribute for more than 4-10 mg/m^2 to the nitrate column. Over the Mediterranean and in Southern Europe, the contribution of coarse nitrates on dust represents about 50% of the calculated total nitrate column. The contribution of nitrates on sea-salt is lower and generally close to 0.5 mg/m^2 over the continents. It only reaches 1 mg/m^2 in localized areas, in particular off the coast of the Eastern US, or over the Mediterranean where both pollution and sea-salt particle are present.

Comparison with measurements

Figure S4 compares the simulated and measured surface concentrations of $SO_4^{=}$, NH_4^{+}, and NO_3^{-} from the EBAS database at NILU. EBAS holds data from EMEP (emep.int), from the US National Atmospheric Deposition Program/National Trend Network (NADP/NTN; http://nadp.sws.uiuc.edu/NTN), from the US Inter- agency Monitoring of Protected Visual Environments (IMPROVE; http://vista.cira.colostate.edu/IMPROVE), from the Clean Air Status and Trends Network (CASTNET; http: //java.epa.gov/castnet) and the EANET, Data on the Acid Deposition in the East Asian Region (http://www.eanet.cc/). These comparisons have been prepared using the AEROCOM evaluation tools (Schulz et al., 2006). The aerosols measurements are mostly from the CASTNET/IMPROVE network over Northern America, from the EMEP network in Europe. This evaluation is performed for the year 2006 based on matching daily mean data, averaged to monthly means.

To obtain a large spatial coverage with respect to evaluation of nitrate and ammonium model values we have included measurements from different methods. These use different combinations of filterpacks and denuders. Little harmonization of the methods has been

achieved globally and there is virtually no choice to pick just one method. Depending on filter type, sampling set-up, temperature and changing ambient conditions during a sampling interval considerable sampling artefacts may occur. At higher temperatures, evaporation of ammonium nitrate from filters has been shown to lead to losses of up to 50% in summer conditions (Vecchi et al., 2009; Sickles and Shadwick, 2002; Allegrini et al., 1994; Yu et al., 2005, Hering and Cass, 1999; Chow et al., 2005, Ashbaugh and Elfred, 2004, Schaap et al., 2004, Schaap et al., 2002). Such sampling artefacts may explain in total a positive model bias, while negative model bias clearly points to model errors. We do not find a clear north-south gradient in bias, neither in Europe nor in Northen America, higher temperatures in the south are not associated with higher positive model bias. However, in central Europe there are several sites, where the positive bias of the model is high in summer and almost absent in winter. In depth inspection of nitrate bias on a map and per measurement site may be accessed via the AeroCom web interface (http://aerocom.met.no/cgi-bin/aerocom/surfobs_annualrs.pl?PROJECT=INCA &Run0=LOI_DH10n&Parameter0=SCONC_NO3).

Figure S5 compares the wet deposition of SO_x (=SO_2+$SO_4^{=}$), NH_x (=NH_3+NH_4^{+}), and NO_y (=NO+NO_2+NO_3+HNO_2+HNO_3+HNO_4+2N_2O_5+PAN+organic nitrates+particulate NO_3^{-}) calculated by the model with the measurements from the EMEP network over Europe, from the NADP network over Northern America and from the EANET network over Eastern Asia.

Figure S6 present an evaluation of the calculated total AOD by comparing with the measurements from the AERONET network (Holben et al., 2001, Kinne et al., 2006). Matching daily data from the model and Aeronet were aggregated to monthly averages. Worldwide, the measured and modeled AOD show a relatively good correlation (R=0.57). The arithmetic mean for the measurements of 0.226 is however underestimated by the modeled values of 0.202 with a Normalized Mean Bias (NMB) of -11%. A good agreement with the AERONET measurements is obtained over Northern America. Over this region the model slightly underestimates the measurements (NMB=-4.5%, R=0.77). Over Africa, higher AOD associated with dust aerosols are calculated. A fairly good correlation is reached (R=0.66) with also a light underestimate by the model of -10%. Over Eastern Asia, the model underestimate the AOD (NMB=-39%). Over Europe, the model slightly overestimates the measurements (NMB=+6%).

Future evolution of atmospheric composition and surface deposition

Figure S7 shows the change in NH_3 surface concentration from the present-day levels in 2030 and 2100 for both RCP4.5 and RCP8.5 (see Fig. 6 from the manuscript for the reference level). For RCP8.5 a significant increase is calculated everywhere in 2030 and 2100 except in Indonesia where biomass burning emissions are reduced. In the central United States, Northern and central Europe, India and China, NH_3 increases by up to 2 $\mu g/cm^3$ in 2100. For the RCP4.5 scenario, a significant increase is still predicted in India and in China where emissions are still predicted to rise. However, concentrations are significantly reduced in Western and Eastern Europe by up to 1 $\mu g/cm^3$ and a lesser increase of 0.5-1 $\mu g/cm^3$ is calculated in the central US. Figure S8 shows the corresponding change in HNO_3 surface concentrations. Due to a reduction in NO_x emissions, HNO_3 has already significantly decreased in 2030 in Northern America and Europe in both scenarios. In contrast, a strong increase is calculated in India and in China reaching more than 2 $\mu g/cm^3$ in 2030. In 2100, the HNO_3 reduction is almost generalized over the continents with the exception of biomass burning regions in Africa and India in the case of RCP8.5. Figure S9 shows the change in $SO_4^=$ surface concentration in 2030 and 2100 for both RCP8.5 and RCP4.5. The concentration increases in India and Southeast Asia by more than 2 $\mu g/cm^3$ in 2030. As expected from the sharp decrease in SO_2 emissions, at the end of the XXIst century, a general decrease of the surface concentration is calculated, reaching more than 2 $\mu g/cm^3$ in Northern America, Europe, and China. As a result of these changes in nitrate precursor surface concentrations, nitrate particles are expected to undergo significant variations in the future. Figure S10, shows the evolution of nitrate particles surface concentrations for 2030 and 2010 and for scenarios RCP8.5 and RCP4.5. The surface concentration increases in India and Southeast Asia by more than 2 $\mu g/cm^3$ in 2030. As a consequence of the sharp decrease in HNO_3 concentrations, a decrease of the surface concentration is calculated, reaching more than 2 $\mu g/cm^3$ in Northern America and Europe in 2030 and 2100. This decrease in surface nitrate concentrations also occurs in China in 2100.

Figure S11, shows the change from the present-day (see Fig. 4 from the main paper for reference levels) of the nitrate column in 2030 and 2100 for the two extremes scenarios RCP4.5 and RCP8.5. The change in nitrate precursors is responsible for a strong increase of the nitrate column in the northern hemisphere. The strong decrease in nitrate surface concentrations calculated over Europe and China in 2030 and 2100 dominates the change in the column which decreases by up to 2 mg/m^2 over these regions.

Figure S12 shows the evolution of the total nitrogen deposition averaged over various regions of the world. The total NO_y + NH_x (wet + dry) deposition is presented. In Europe and Northern America, the total N deposition slightly decreases or remains close to its present-day value in the case of scenario RCP8.5. In Asia and India, the NO_y deposition generally increases in 2030 or 2050 due to higher NO_x emissions in these regions before decreasing at the end of the XXIst century. In addition, the NH_x deposition generally increases during the course of the century to reach maximum values in 2100. Figure S13 shows that the fraction of N deposited as NH_x increases from about 60% to 80% in these regions. The same tendency is found over oceanic regions and globally. The total N deposited remains fairly stable or slightly decreases in these regions during the XXIst century but the fraction of N deposited as NH_x increases from 45% to 55-70% over the ocean and from 55% to 70-80% globally.

References

Allegrini, I., A. Febo, C. Perrino and P. Masia, Measurement of Atmospheric Nitric-Acid in Gas-Phase and Nitrate in Particulate Matter by Means of Annular Denuders, *International Journal of Environmental Analytical Chemistry*, 54, 183-201, 1994.

Ashbaugh, L. L. and R. A. Eldred, Loss of Particle Nitrate from Teflon Sampling Filters: Effects on Measured Gravimetric Mass in California and in the Improve Network, *Journal of the Air & Waste Management Association,* 54, 93-104, 2004.

Chow, J. C., J. G. Watson, D. H. Lowenthal and K. L. Magliano, Loss of Pm2.5 Nitrate from Filter Samples in Central California, *Journal of the Air & Waste Management Association* 55, 1158-1168, 2005.

Dall'Osto, M., R. M. Harrison, H. Coe, P. I. Williams, and J. D. Allan, Real time chemical characterization of local and regional nitrate aerosols, Atmos. Chem. Phys., 9, 3709-3720, 2009.

Hering, S. and G. Cass, The Magnitude of Bias in the Measurement of Pm2.5 Arising from Volatilization of Particulate Nitrate from Teflon Filters, *Journal of the Air & Waste Management Association*, 49, 725-733, 1999..

Mozurkewich, M., The dissociation constant of ammonium nitrate and its dependence on temperature, relative humidity and particle size, *Atmos. Environ.*, 27A, 261-270, 1993.

Nenes, A., S. Pandis, and C. Pilinis, ISORROPIA: a new thermodynamic equilibrium model for multiphase multicomponent inorganic aerosols, *Aquat. Geochem.*, 4, 123-152, 1998.

Schaap, M., K. Muller and H. M. ten Brink, Constructing the European Aerosol Nitrate Concentration Field from Quality Analysed Data, *Atmospheric Environment,* 36, 1323-1335, 2002.

Schaap, M., G. Spindler, M. Schulz, K. Acker, W. Maenhaut, A. Berner, W. Wieprecht, N. Streit, K. Muller, E. Bruggemann, X. Chi, J. P. Putaud, R. Hitzenberger, H. Puxbaum, U. Baltensperger and H. ten Brink, Artefacts in the Sampling of Nitrate Studied in the Intercomp Campaigns of Eurotrac-Aerosol, Atmospheric Environment, 38, 6487-6496, 2004.

Seinfeld, J. H., and S. N. Pandis, *Atmospheric chemistry and Physics*, John Wiley and Sons, New York, 1998.

203 Sickles, J. E. and D. S. Shadwick, Biases in Clean Air Status and Trends Network Filter Pack
204 Results Associated with Sampling Protocol, *Atmospheric Environment*, 36, 4687-4698, 2002.

205 Vecchi, R., G. Valli, P. Fermo, A. D'Alessandro, A. Piazzalunga and V. Bernardoni, Organic
206 and Inorganic Sampling Artefacts Assessment, *Atmospheric Environment*, 43, 1713-1720,
207 2009.

208 Yu, X. Y., L. Taehyoung, B. Ayres, S. M. Kreidenweis, J. L. Collett and W. Maim.
209 Particulate Nitrate Measurement Using Nylon Filters, *Journal of the Air & Waste*
210 *Management Association,* 55, 1100-1110, 2005.

211

Figure Captions

Figure S1. Variation of NO_3^- (blue) and NH_4^+ (red) equilibrium concentrations ($\mu g/m^3$) as a function of total sulfate, total ammonia, total nitrate ($\mu g/m^3$), relative humidity (%) and temperature (T). INCA model results : solid line, ISORROPIA model: triangles.

Figure S2. Simulated diurnal variation of NO_3^- surface concentration ($\mu g/m^3$) during the 1/08/2009 to 30/10/2009 period in England, the Po valley, The Netherlands, and in Northern China.

Figure S3. Annual mean tropospheric column of (top) fine mode nitrate aerosols, (middle) coarse mode nitrates on dust, and (bottom) coarse mode nitrates on sea-salt simulated for present-day conditions (mg/m^2).

Figure S4. Simulated surface concentration of sulfates ($\mu S/m^3$), ammonium ($\mu N/m^3$), and nitrates ($\mu N/m^3$) for the year 2006 compared to EBAS data over the world (top row), Europe (middle) and Northern America (bottom). Dashed lines indicate 1:2 and 2:1 ratios.

Figure S5. Simulated SO_x ($gS/m^2/yr$), NH_x and NO_y ($gN/m^2/yr$) wet deposition for the year 2006 compared to EBAS data for the world, over Europe, Northern America, and Eastern Asia. Dashed lines indicate 1:2 and 2:1 ratios.

Figure S6. Simulated total aerosol optical depth at 550 nm for the year 2006 compared to the AERONET data worldwide, over Europe, Northern America, Northern Africa, and Eastern Asia. Dashed lines indicate 1:2 and 2:1 ratios.

Figure S7. Changes in ammonia surface concentration (μg/m^3) relative to the present-day distribution for scenario RCP8.5 (top) and RCP4.5 (bottom) calculated for 2030 (left) and 2100 (right).

Figure S8. Changes in nitric acid surface concentration (μg/m^3) relative to the present-day distribution for scenario RCP8.5 (top) and RCP4.5 (bottom) calculated for 2030 (left) and 2100 (right).

Figure S9. Changes in sulfate surface concentration (μg/m^3) relative to the present-day distribution for scenario RCP8.5 (top) and RCP4.5 (bottom) calculated for 2030 (left) and 2100 (right).

Figure S10. Changes in nitrate surface concentration (μg/m^3) relative to the present-day distribution for scenario RCP8.5 (top) and RCP4.5 (bottom) calculated for 2030 (left) and 2100 (right).

Figure S11. Changes in nitrate column (mg/m^2) relative to the present-day distribution for scenario RCP8.5 (top) and RCP4.5 (bottom) calculated for 2030 (left) and 2100 (right).

Figure S12. Evolution of NH_x+NO_y total deposition (mgN/m^2/yr) for scenario RCP8.5 (red), RCP6.0 (yellow), RCP4.5 (green) and RCP2.6 (blue) between present-day and 2100. The averaged deposition is depicted for Europe, Northern America, Northern Asia, Southern Asia, India, Africa, Southern America, Australia, the global ocean, and the globe.

Figure S13. Evolution of the NH_x fractional contribution to NH_x+NO_y total deposition (%) for scenario RCP8.5 (red), RCP6.0 (yellow), RCP4.5 (green) and RCP2.6 (blue) between present-day and 2100. The averaged deposition is depicted for Europe, Northern America, Northern

Asia, Southern Asia, India, Africa, Southern America, Australia, the global ocean, and the globe.

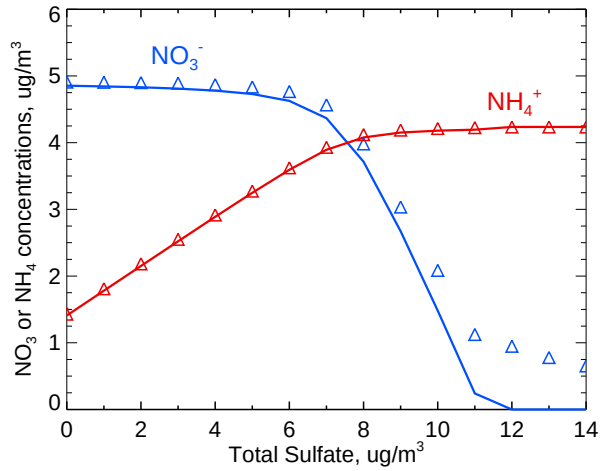
NO3-
NH4+
NO3 or NH4 concentrations, ug/m3
Total Sulfate, ug/m3

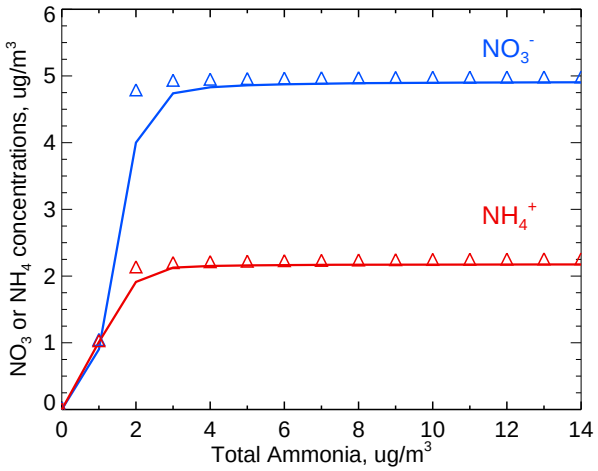
NO3-
NH4+
NO3 or NH4 concentrations, ug/m3
Total Ammonia, ug/m3

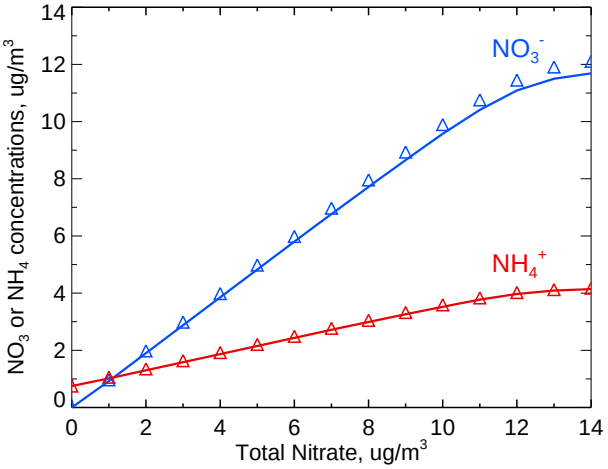
NO3-
NH4+
NO3 or NH4 concentrations, ug/m3
Total Nitrate, ug/m3

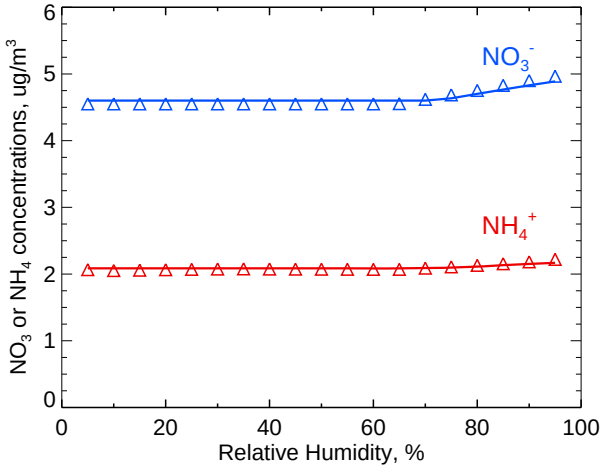
NO3-
NH4+
NO3 or NH4 concentrations, ug/m3
Relative Humidity, %

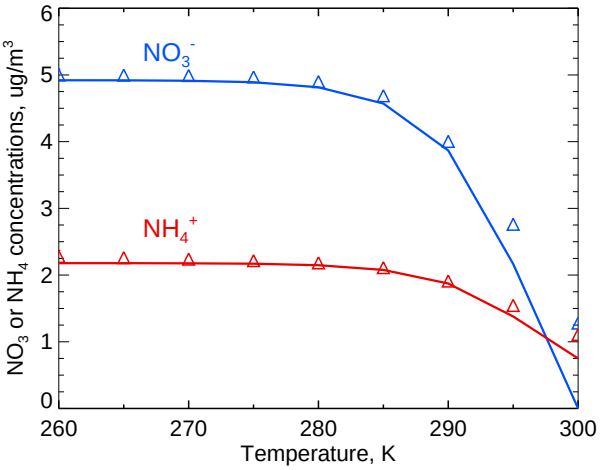
NO3-
NH4+
NO3 or NH4 concentrations, ug/m3
Temperature, K

Figure S1

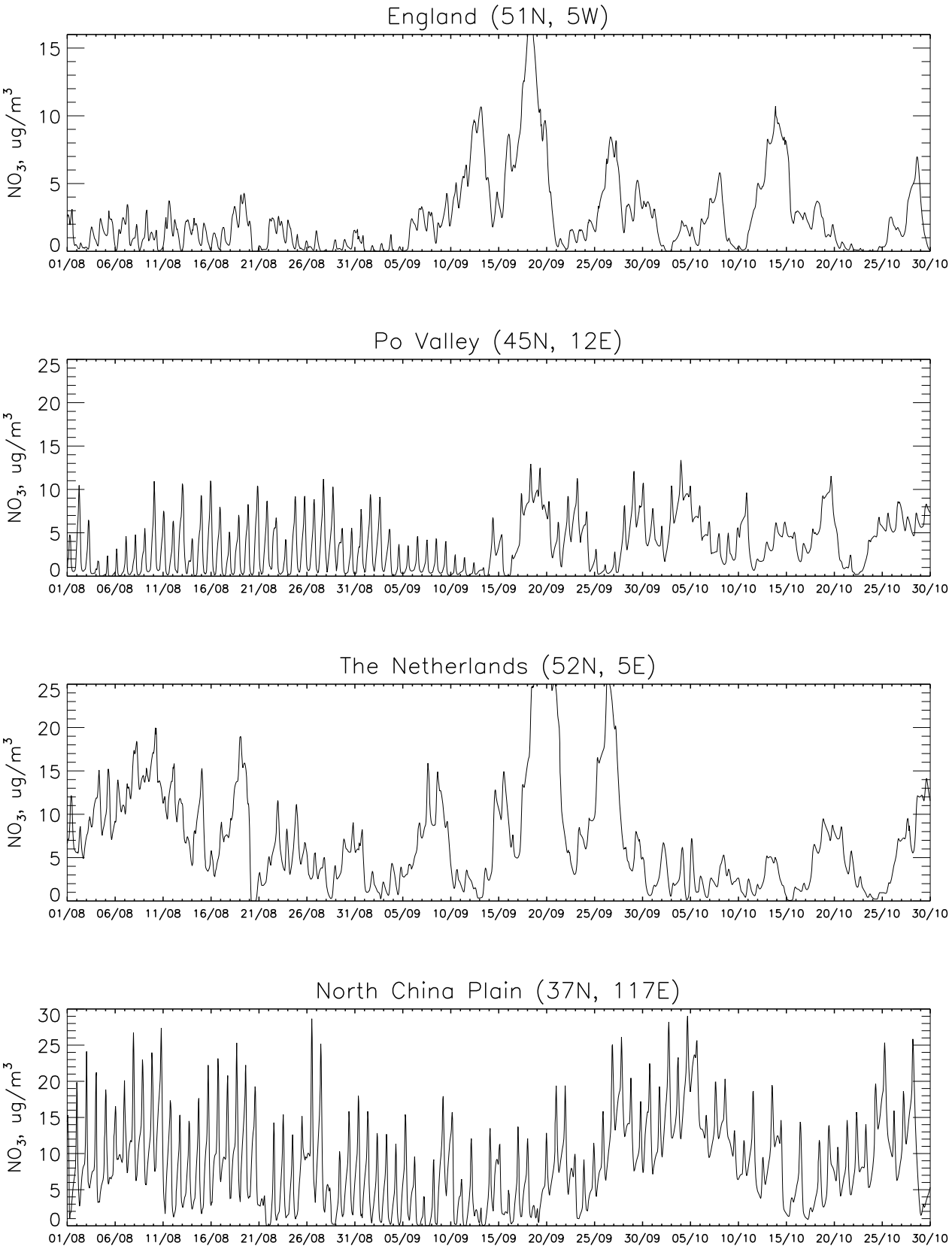
England (51N, 5W)
Po Valley (45N, 12E)
The Netherlands (52N, 5E)
North China Plain (37N, 117E)
NO3, ug/m3
01/08 06/08 11/08 16/08 21/08 26/08 31/08 05/09 10/09 15/09 20/09 25/09 30/09 05/10 10/10 15/10 20/10 25/10 30/10

Figure S2

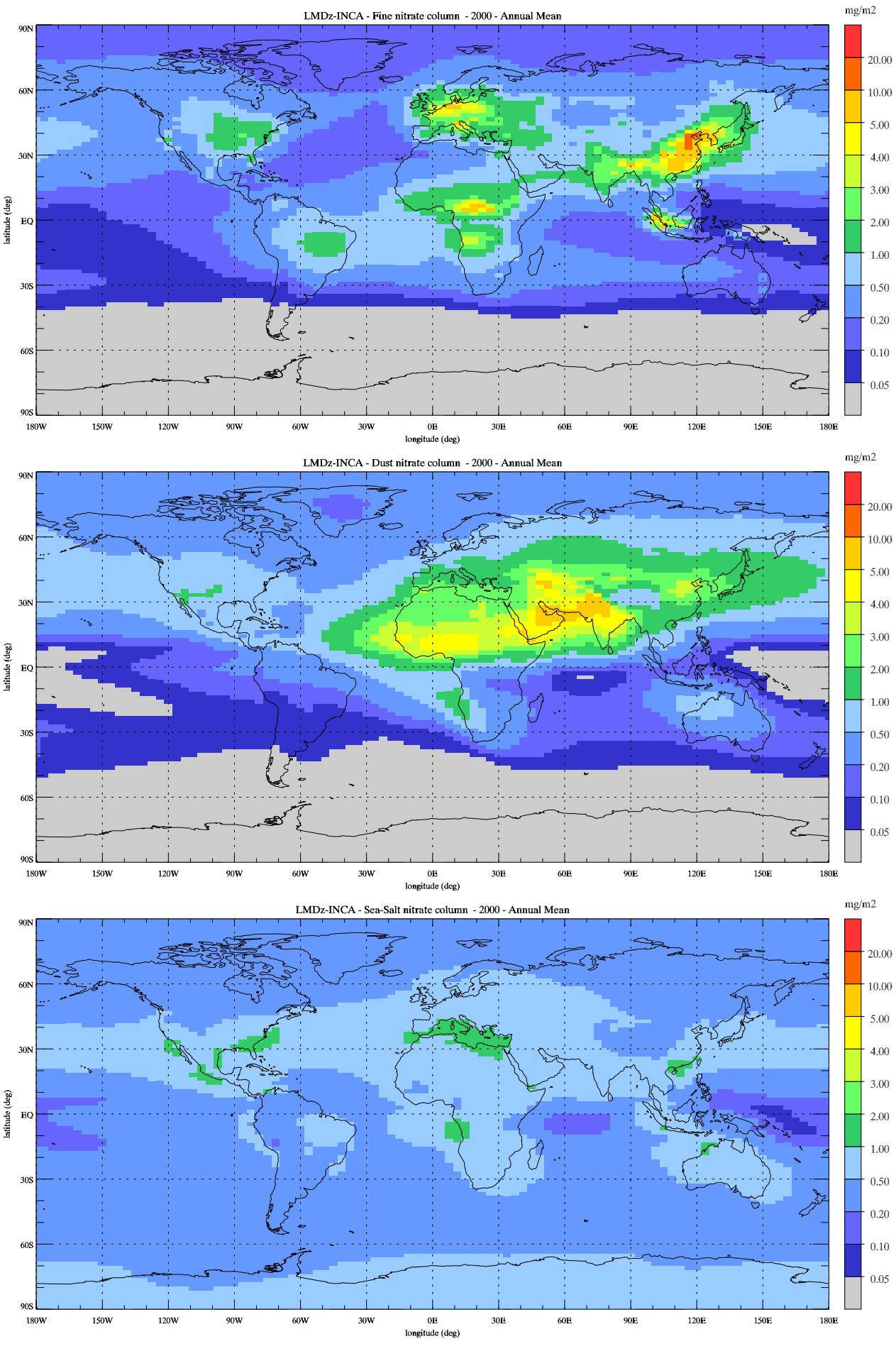
LMDz-INCA - Fine nitrate column - 2000 - Annual Mean
LMDz-INCA - Dust nitrate column - 2000 - Annual Mean
LMDz-INCA - Sea-Salt nitrate column - 2000 - Annual Mean
mg/m2
20.00
10.00
5.00
4.00
3.00
2.00
1.00
0.50
0.20
0.10
0.05
90N
60N
30N
EQ
30S
60S
90S
latitude (deg)
180W
150W
120W
90W
60W
30W
0E
30E
60E
90E
120E
150E
180E
longitude (deg)

Figure S3

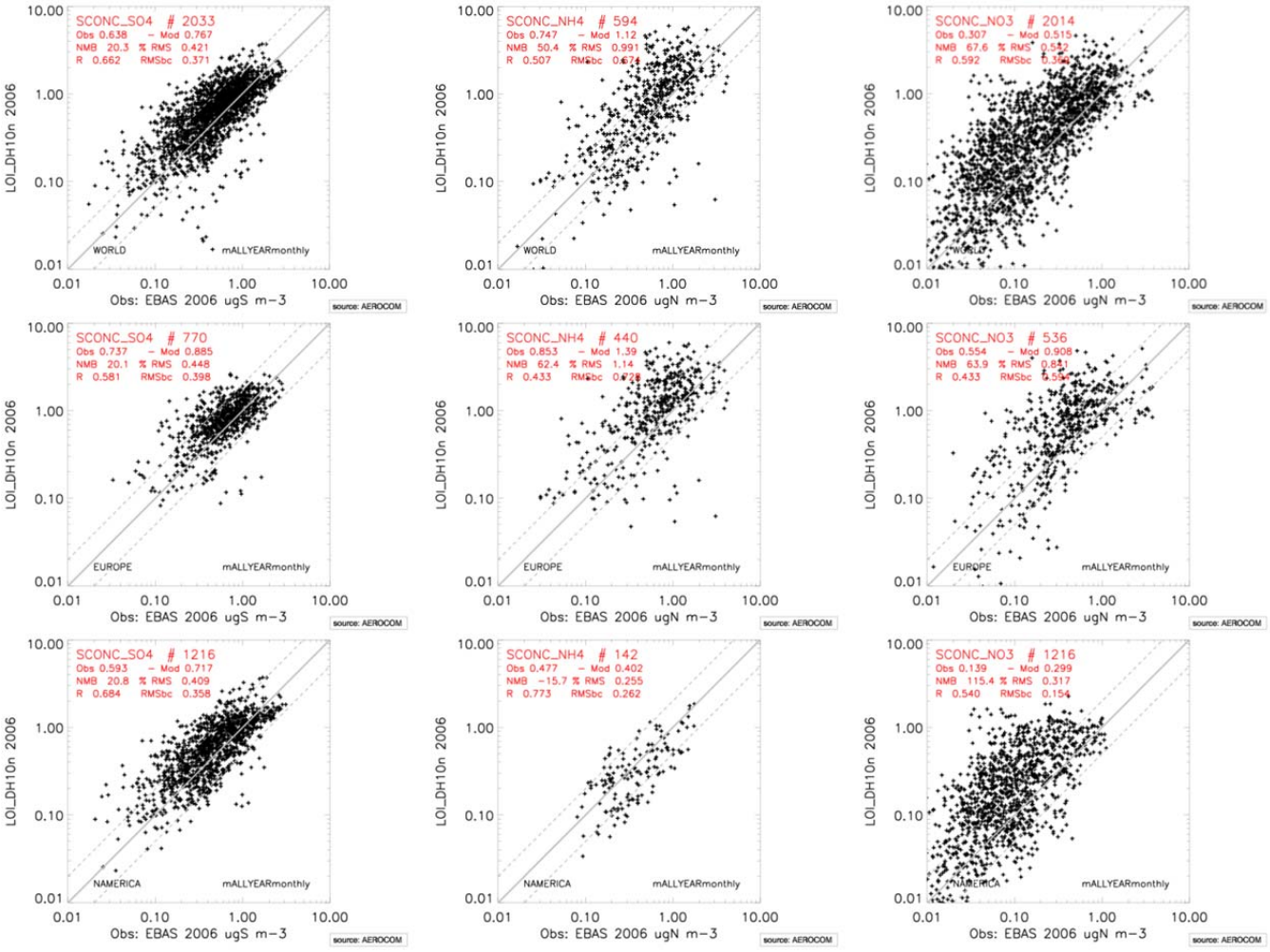
SCONC_SO4 # 2033
Obs 0.638 – Mod 0.767
NMB 20.3 % RMS 0.421
R 0.662 RMSbc 0.371
WORLD
mALLYEARmonthly
LOI_DH10n 2006
Obs: EBAS 2006 ugS m-3
source: AEROCOM
SCONC_NH4 # 594
Obs 0.747 – Mod 1.12
NMB 50.4 % RMS 0.991
R 0.507 RMSbc 0.674
WORLD
mALLYEARmonthly
Obs: EBAS 2006 ugN m-3
source: AEROCOM
SCONC_NO3 # 2014
Obs 0.307 – Mod 0.515
NMB 67.6 % RMS 0.532
R 0.592 RMSbc 0.364
WORLD
Obs: EBAS 2006 ugN m-3
source: AEROCOM
SCONC_SO4 # 770
Obs 0.737 – Mod 0.885
NMB 20.1 % RMS 0.448
R 0.581 RMSbc 0.398
EUROPE
mALLYEARmonthly
Obs: EBAS 2006 ugS m-3
source: AEROCOM
SCONC_NH4 # 440
Obs 0.853 – Mod 1.39
NMB 62.4 % RMS 1.14
R 0.433 RMSbc 0.928
EUROPE
mALLYEARmonthly
Obs: EBAS 2006 ugN m-3
source: AEROCOM
SCONC_NO3 # 536
Obs 0.554 – Mod 0.908
NMB 63.9 % RMS 0.851
R 0.433 RMSbc 0.594
EUROPE
mALLYEARmonthly
Obs: EBAS 2006 ugN m-3
source: AEROCOM
SCONC_SO4 # 1216
Obs 0.593 – Mod 0.717
NMB 20.8 % RMS 0.409
R 0.684 RMSbc 0.358
NAMERICA
mALLYEARmonthly
Obs: EBAS 2006 ugS m-3
source: AEROCOM
SCONC_NH4 # 142
Obs 0.477 – Mod 0.402
NMB -15.7 % RMS 0.255
R 0.773 RMSbc 0.262
NAMERICA
mALLYEARmonthly
Obs: EBAS 2006 ugN m-3
source: AEROCOM
SCONC_NO3 # 1216
Obs 0.139 – Mod 0.299
NMB 115.4 % RMS 0.317
R 0.540 RMSbc 0.154
NAMERICA
mALLYEARmonthly
Obs: EBAS 2006 ugN m-3
source: AEROCOM

Figure S4

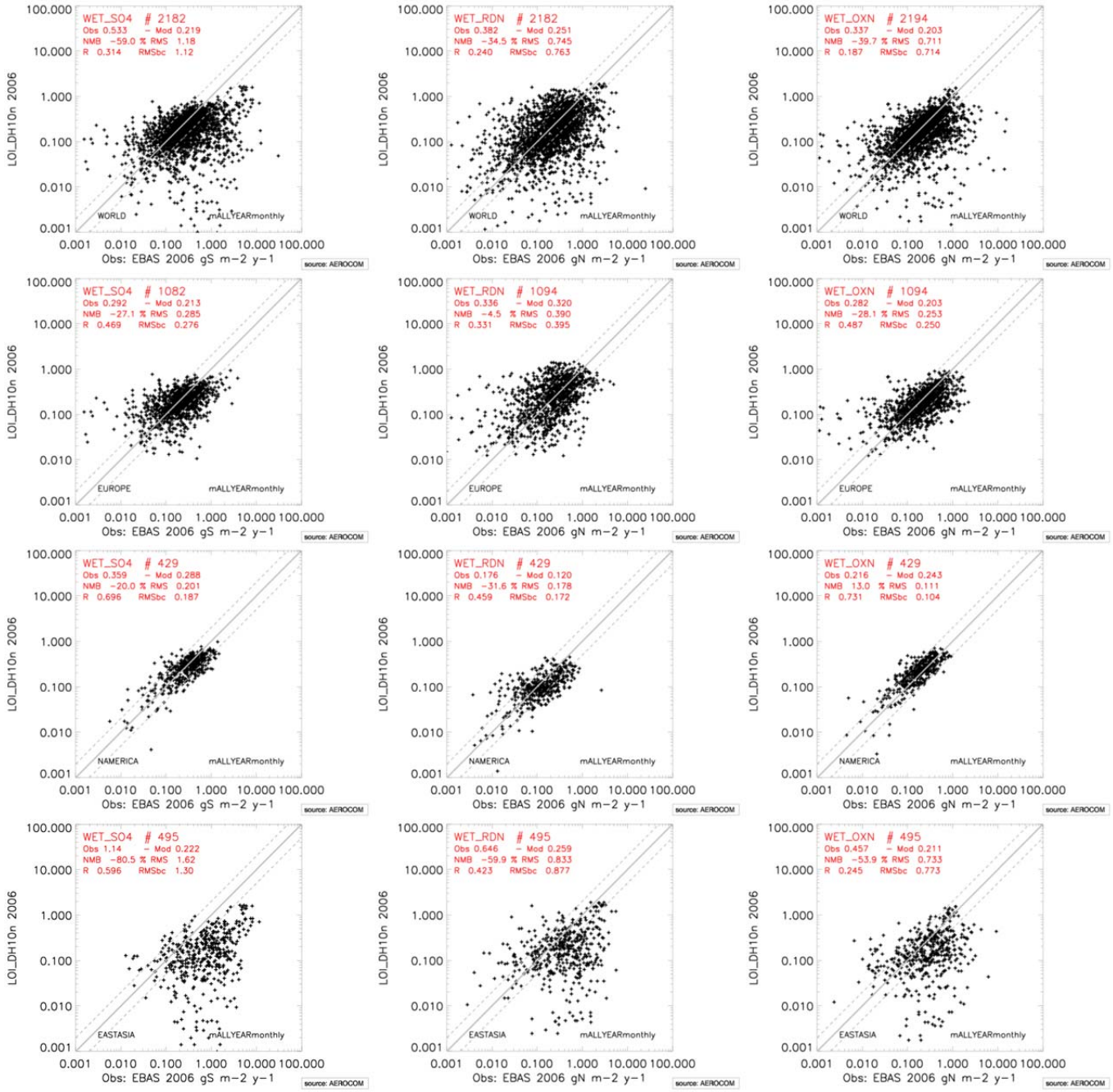
WET_SO4 # 2182
Obs 0.533 – Mod 0.219
NMB −59.0 % RMS 1.18
R 0.314 RMSbc 1.12
WET_RDN # 2182
Obs 0.382 – Mod 0.251
NMB −34.5 % RMS 0.745
R 0.240 RMSbc 0.763
WET_OXN # 2194
Obs 0.337 – Mod 0.203
NMB −39.7 % RMS 0.711
R 0.187 RMSbc 0.714
WET_SO4 # 1082
Obs 0.292 – Mod 0.213
NMB −27.1 % RMS 0.285
R 0.469 RMSbc 0.276
WET_RDN # 1094
Obs 0.336 – Mod 0.320
NMB −4.5 % RMS 0.390
R 0.331 RMSbc 0.395
WET_OXN # 1094
Obs 0.282 – Mod 0.203
NMB −28.1 % RMS 0.253
R 0.487 RMSbc 0.250
WET_SO4 # 429
Obs 0.359 – Mod 0.288
NMB −20.0 % RMS 0.201
R 0.696 RMSbc 0.187
WET_RDN # 429
Obs 0.176 – Mod 0.120
NMB −31.6 % RMS 0.178
R 0.459 RMSbc 0.172
WET_OXN # 429
Obs 0.216 – Mod 0.243
NMB 13.0 % RMS 0.111
R 0.731 RMSbc 0.104
WET_SO4 # 495
Obs 1.14 – Mod 0.222
NMB −80.5 % RMS 1.62
R 0.596 RMSbc 1.30
WET_RDN # 495
Obs 0.646 – Mod 0.259
NMB −59.9 % RMS 0.833
R 0.423 RMSbc 0.877
WET_OXN # 495
Obs 0.457 – Mod 0.211
NMB −53.9 % RMS 0.733
R 0.245 RMSbc 0.773
LOI_DH10n 2006
Obs: EBAS 2006 gS m−2 y−1
Obs: EBAS 2006 gN m−2 y−1
WORLD
EUROPE
NAMERICA
EASTASIA
mALLYEARmonthly
source: AEROCOM

Figure S5

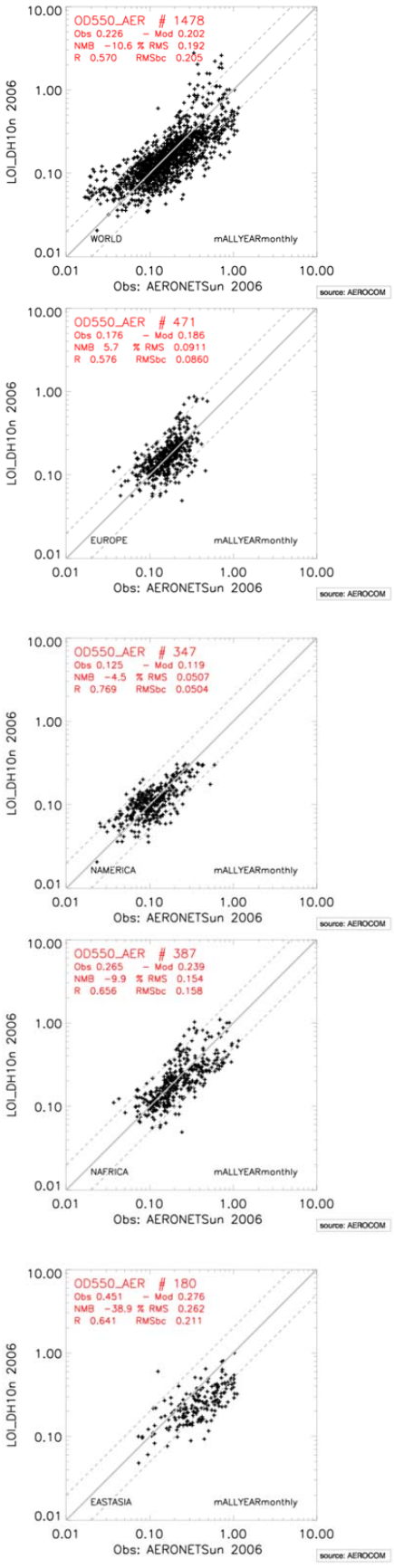
OD550_AER # 1478
Obs 0.226 ~ Mod 0.202
NMB -10.6 % RMS 0.192
R 0.570 RMSbc 0.205
WORLD
mALLYEARmonthly
OD550_AER # 471
Obs 0.176 ~ Mod 0.186
NMB 5.7 % RMS 0.0911
R 0.576 RMSbc 0.0860
EUROPE
mALLYEARmonthly
OD550_AER # 347
Obs 0.125 ~ Mod 0.119
NMB -4.5 % RMS 0.0507
R 0.769 RMSbc 0.0504
NAMERICA
mALLYEARmonthly
OD550_AER # 387
Obs 0.265 ~ Mod 0.239
NMB -9.9 % RMS 0.154
R 0.656 RMSbc 0.158
NAFRICA
mALLYEARmonthly
OD550_AER # 180
Obs 0.451 ~ Mod 0.276
NMB -38.9 % RMS 0.262
R 0.641 RMSbc 0.211
EASTASIA
mALLYEARmonthly
LOI_DH10n 2006
Obs: AERONETSun 2006
0.01
0.10
1.00
10.00
source: AEROCOM

Figure S6

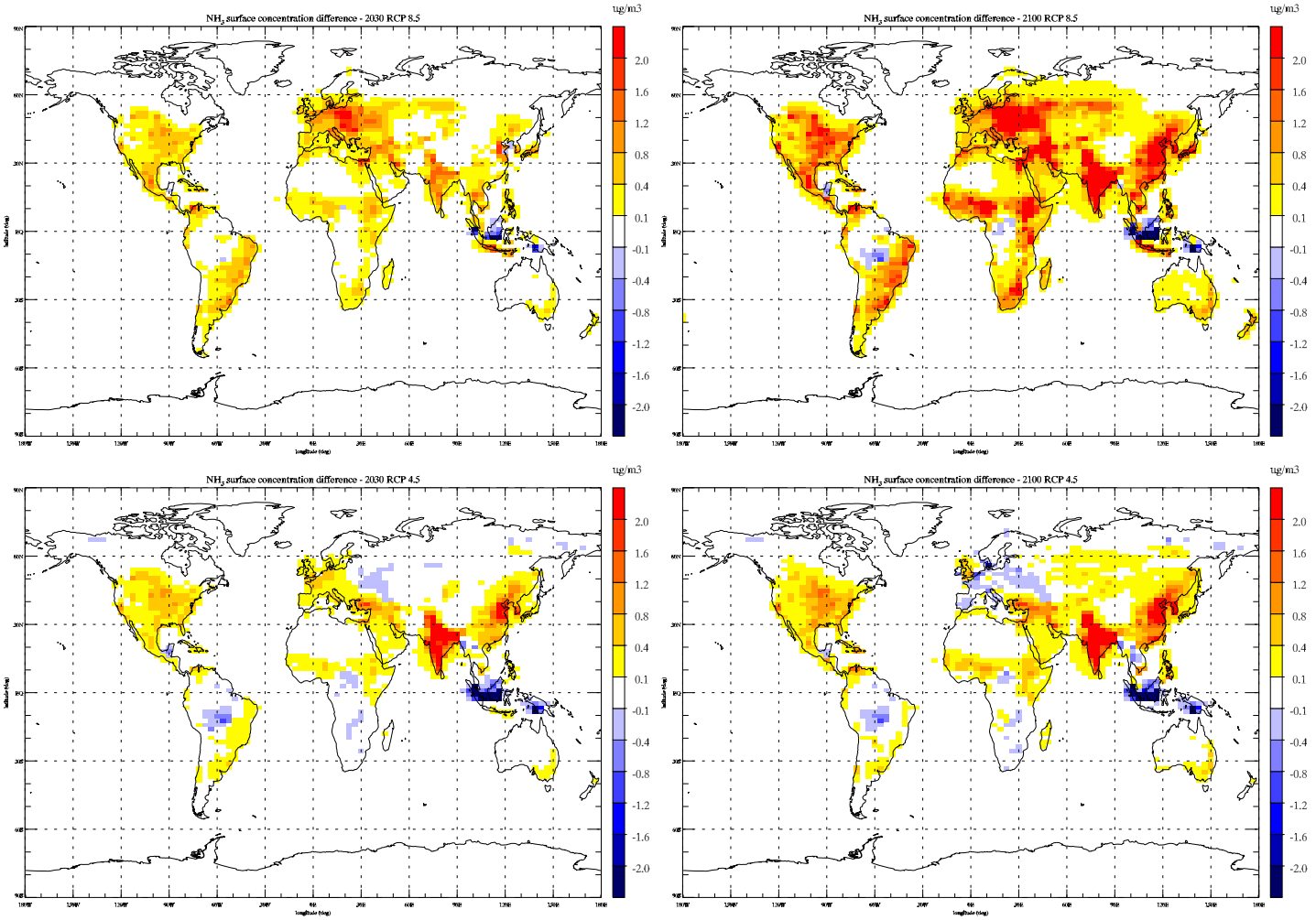
NH3 surface concentration difference - 2030 RCP 8.5
NH3 surface concentration difference - 2100 RCP 8.5
NH3 surface concentration difference - 2030 RCP 4.5
NH3 surface concentration difference - 2100 RCP 4.5
ug/m3
2.0
1.6
1.2
0.8
0.4
0.1
-0.1
-0.4
-0.8
-1.2
-1.6
-2.0

Figure S7

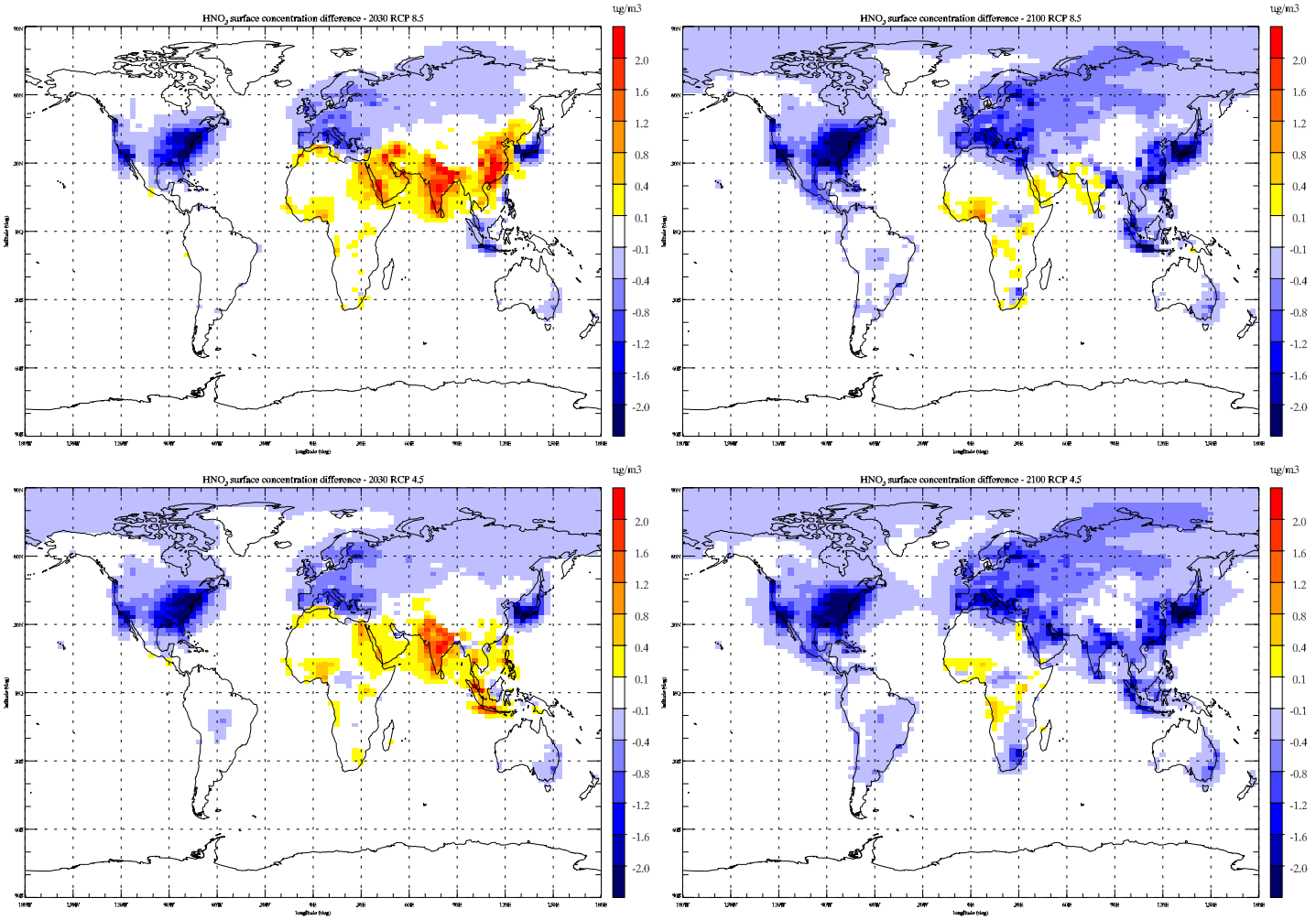
HNO3 surface concentration difference - 2030 RCP 8.5
HNO3 surface concentration difference - 2100 RCP 8.5
HNO3 surface concentration difference - 2030 RCP 4.5
HNO3 surface concentration difference - 2100 RCP 4.5
ug/m3
2.0
1.6
1.2
0.8
0.4
0.1
-0.1
-0.4
-0.8
-1.2
-1.6
-2.0

Figure S8

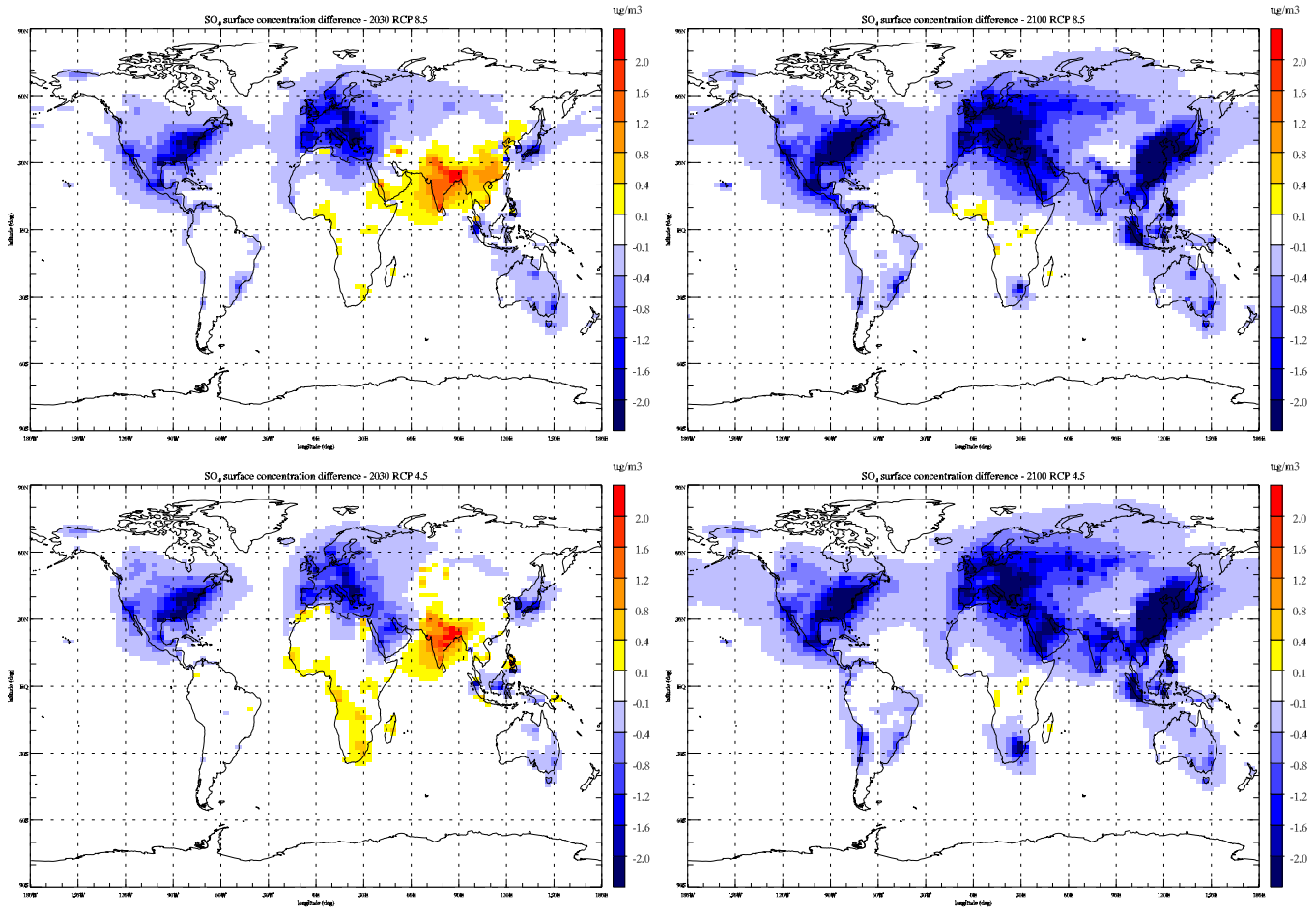
SO4 surface concentration difference - 2030 RCP 8.5
SO4 surface concentration difference - 2100 RCP 8.5
SO4 surface concentration difference - 2030 RCP 4.5
SO4 surface concentration difference - 2100 RCP 4.5
ug/m3
2.0
1.6
1.2
0.8
0.4
0.1
-0.1
-0.4
-0.8
-1.2
-1.6
-2.0

Figure S9

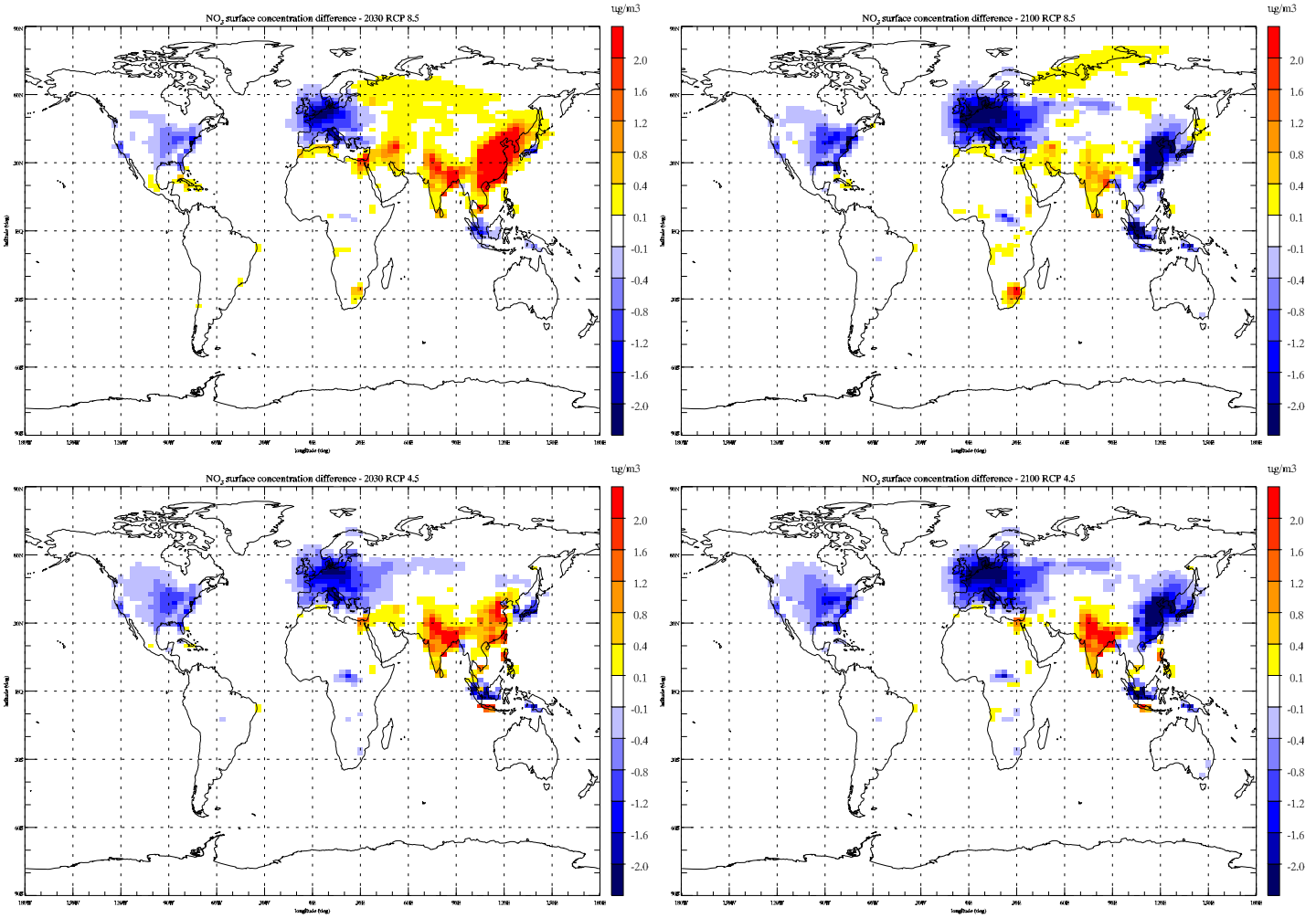
NO2 surface concentration difference - 2030 RCP 8.5
NO2 surface concentration difference - 2100 RCP 8.5
NO2 surface concentration difference - 2030 RCP 4.5
NO2 surface concentration difference - 2100 RCP 4.5
ug/m3
2.0
1.6
1.2
0.8
0.4
0.1
-0.1
-0.4
-0.8
-1.2
-1.6
-2.0

Figure S10

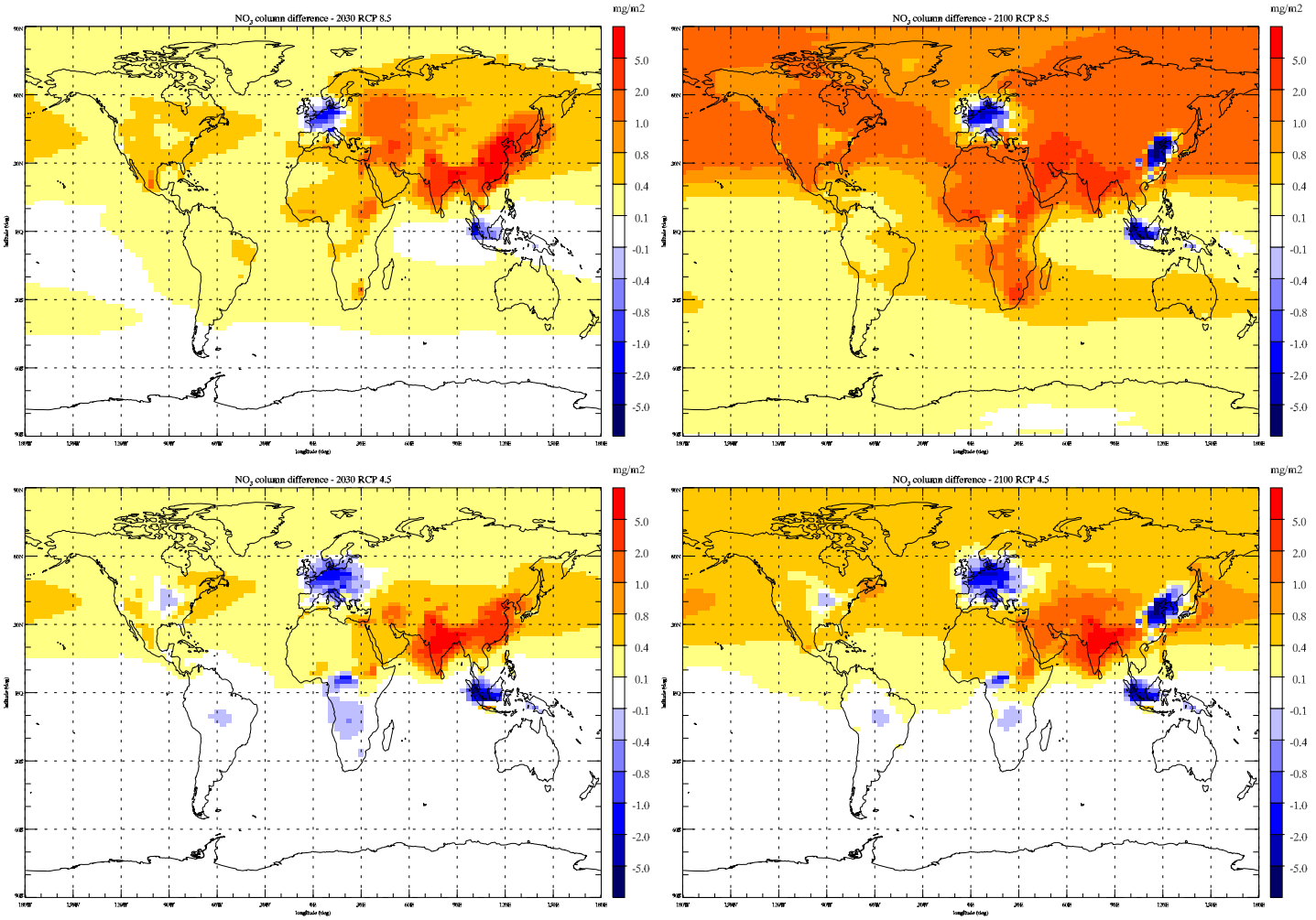
NO2 column difference - 2030 RCP 8.5
NO2 column difference - 2100 RCP 8.5
NO2 column difference - 2030 RCP 4.5
NO2 column difference - 2100 RCP 4.5
mg/m2
5.0
2.0
1.0
0.8
0.4
0.1
-0.1
-0.4
-0.8
-1.0
-2.0
-5.0

Figure S11

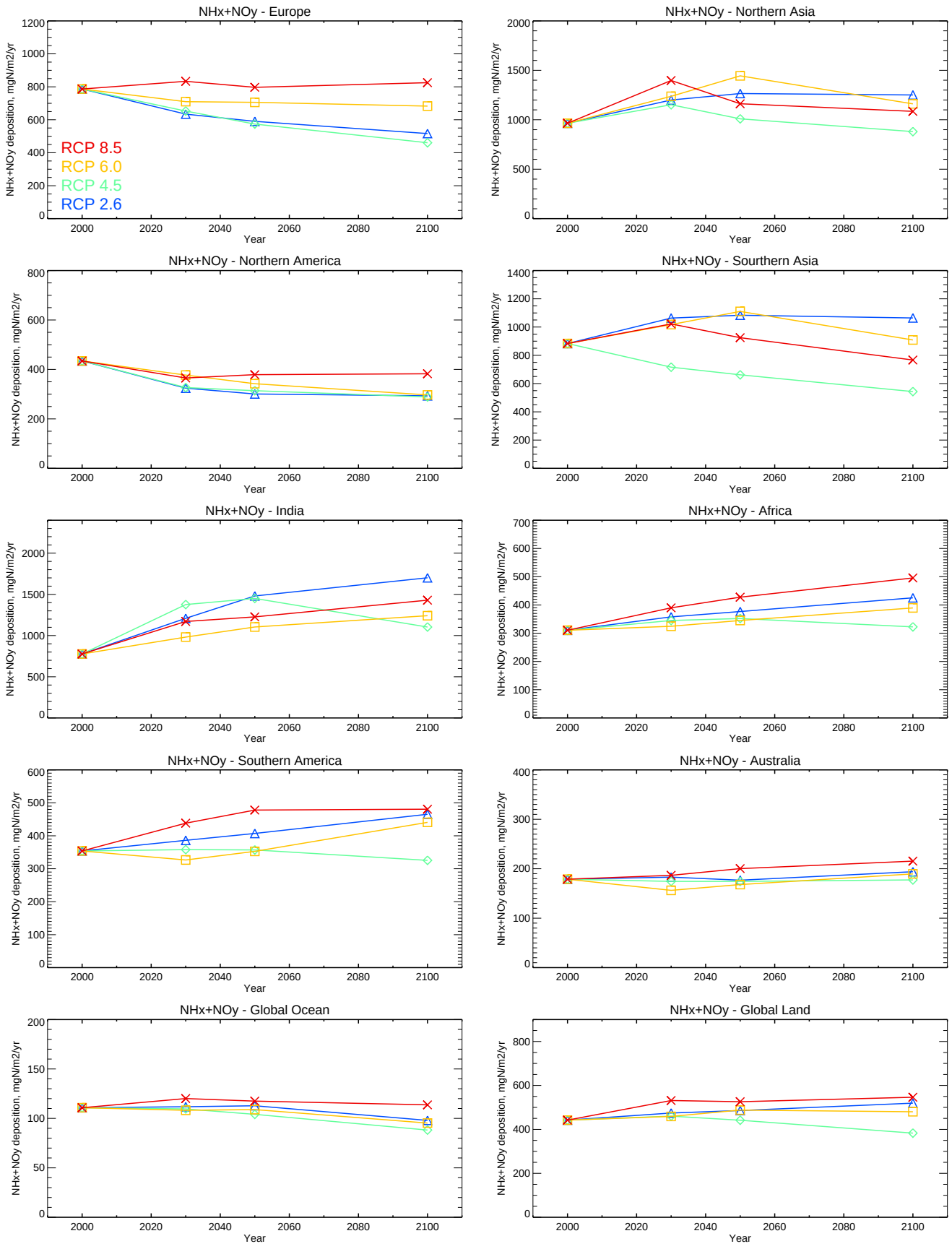
NHx+NOy - Europe
NHx+NOy - Northern Asia
NHx+NOy - Northern America
NHx+NOy - Sourthern Asia
NHx+NOy - India
NHx+NOy - Africa
NHx+NOy - Southern America
NHx+NOy - Australia
NHx+NOy - Global Ocean
NHx+NOy - Global Land
NHx+NOy deposition, mgN/m2/yr
Year
RCP 8.5
RCP 6.0
RCP 4.5
RCP 2.6

Figure S12

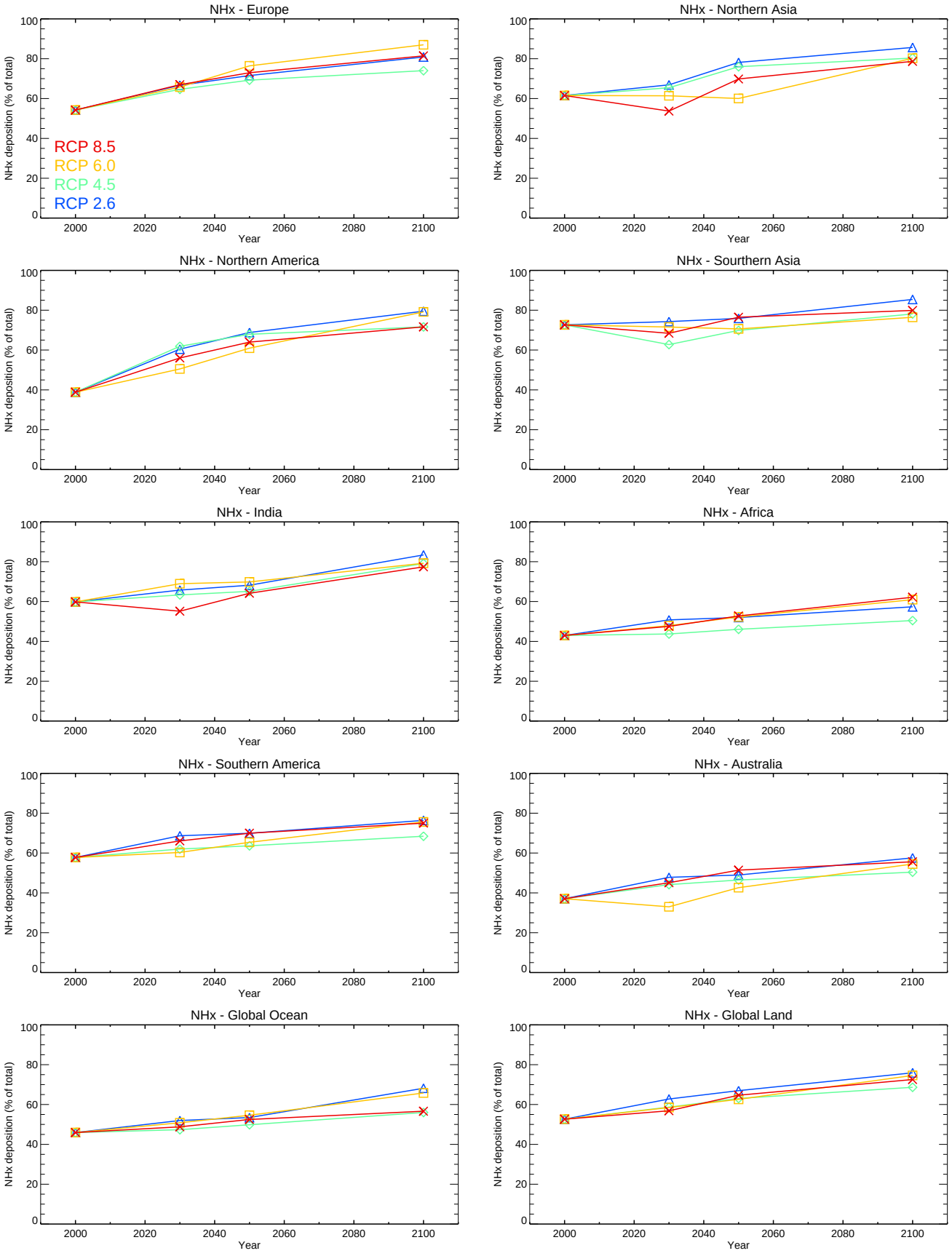
NHx - Europe
NHx - Northern Asia
NHx - Northern America
NHx - Sourthern Asia
NHx - India
NHx - Africa
NHx - Southern America
NHx - Australia
NHx - Global Ocean
NHx - Global Land
NHx deposition (% of total)
Year
RCP 8.5
RCP 6.0
RCP 4.5
RCP 2.6

Figure S13